Remote Sensing of Environment 158 (2015) 465–477

Contents lists available at ScienceDirect

Remote Sensing of Environment

journal homepage: www.elsevier.com/locate/rse

Spatial scaling of reflectance and surface albedo over a mixed-use, temperate forest landscape during snow-covered periods

Elizabeth A. Burakowski [a,*], Scott V. Ollinger [a], Lucie Lepine [a], Crystal B. Schaaf [b], Zhuosen Wang [b], Jack E. Dibb [a], David Y. Hollinger [c], JiHyun Kim [d], Angel Erb [b], Mary Martin [a]

[a] Institute for the Study of Earth, Oceans, and Space, University of New Hampshire, 8 College Road, Durham, NH 03824, USA
[b] School for the Environment, College of Science and Mathematics, University of Massachusetts Boston, 100 Morrissey Blvd, Boston, MA 02125-3393, USA
[c] USDA Forest Service Northern Research Station, 271 Mast Road, Durham, NH 03824, USA
[d] Center for Remote Sensing, Department of Geography and Environment, Boston University, Boston, MA 02115, USA

ARTICLE INFO

Article history:
Received 25 April 2014
Received in revised form 1 November 2014
Accepted 17 November 2014
Available online 12 December 2014

Keywords:
MODIS
Snow
Albedo
Reflectance
Temperate forest
Hyperspectral imagery
Spatial representativeness

ABSTRACT

Albedo products from the MODerate resolution Imaging Spectroradiometer (MODIS) have been validated extensively over spatially homogeneous sites with snow-cover. This study evaluated the spatial scaling of albedo and related reflectance-based quantities over areas of high spatial heterogeneity in temperate mixed forest, deciduous forest, urban and built-up, and cropland/natural mosaic lands under snow covered conditions. Reflectance-based quantities evaluated included spectral radiance, surface directional reflectance, and spectral and broadband albedo derived from ground- and tower-based measurements and high-resolution (5 m) hyperspectral imagery (HSI) to coarse resolution (~500 m) MODIS satellite data.

Our approach first compared ground- and tower-based spectral and broadband reflectance quantities to HSI data, then to evaluate HSI with MODIS reflectance-based products. Over snow-covered pasture, HSI directional reflectance was biased lower than ground-based measurements collected using a spectroradiometer, and greatly underestimated at wavelengths less than 450 nm. Tower-based shortwave broadband albedo (280–2800 nm) and HSI albedo agreed within ±0.04. HSI directional spectral reflectance agreed well with tower-based measurements of spectral albedo collected using a spectroradiometer and remote cosine receptor above a mixed forest canopy with underlying snow cover. Spectral albedo collected over a dormant deciduous broadleaf canopy increased from 0.10 for snow-free conditions to 0.14–0.18 when snow-cover was present under the canopy. Canopy shortwave broadband albedo was not very sensitive to underlying snowpack depth, indicative of strong vegetation masking.

Next, HSI data were spatially aggregated and averaged to 500 m MODIS grids and compared to two MODIS albedo products: (1) MODIS/Terra and Aqua Combined Bidirectional Reflectance Distribution Function (BRDF) Albedo V005 (MCD43A, magnitude inversion), and (2) MODIS/Terra Snow Cover Daily L3 Global 500 m Grid (MOD10A1). An assessment of surface heterogeneity demonstrated that MODIS products generally perform well for snow-covered landscapes with high spatial heterogeneity, with biases between ±0.04 and RMSEs less than 0.085 for mixed and deciduous broadleaf forested and urban & built-up land cover classes, and less than 0.11 for cropland/natural mosaic. Biases were generally lower for MOD10A1 compared to MCD43A3.

Mean shortwave broadband albedo from MODIS and HSI over deciduous broadleaf and mixed forest with underlying snow cover ranged from 0.14 to 0.28. Albedo over MODIS grids characterized as a mosaic of cropland, forests, grasslands, and shrublands (e.g., cropland/natural mosaic) was substantially higher than forested grids under snow-covered conditions, ranging from 0.39 to 0.43.

© 2014 Elsevier Inc. All rights reserved.

1. Introduction

Albedo, the ratio of incoming to reflected solar radiation, plays an important role in climate by regulating the amount of shortwave radiation reflected or absorbed and subsequently reradiated as longwave radiation by a surface. Due to its high albedo, snow cover increases the proportion of solar radiation reflected from the Earth's surface, producing a 1.5 °C to 4.5 °C cooling effect compared to snow-free surfaces (Mote, 2008). The magnitude of cooling depends on a

* Corresponding author at: National Center for Atmospheric Research, 1850 Table Mesa Drive, Boulder, CO 80305, USA. Tel.: +1 603 548 7388.
E-mail addresses: burakows@ncar.edu (E.A. Burakowski), lucie.lepine@unh.edu (L. Lepine), crystal.schaaf@umb.edu (C.B. Schaaf), zhuosen.wang@umb.edu (Z. Wang), jack.dibb@unh.edu (J.E. Dibb), davidh@hypatia.unh.edu (D.Y. Hollinger), jhkim26@bu.edu (J. Kim), Angela.Erb001@umb.edu (A. Erb), mary.martin@unh.edu (M. Martin).

http://dx.doi.org/10.1016/j.rse.2014.11.023
0034-4257/© 2014 Elsevier Inc. All rights reserved.

variety of factors including snow depth, cloud cover solar zenith angle, and land cover type. Land cover type is particularly important because it limits the maximum snow-covered albedo based on the presence or absence of canopy structure. Forest canopies shield highly reflective snow cover, lowering surface albedo in winter and exerting a positive climate forcing (e.g., warming) relative to non-forested lands covered with snow (Bonan, 2008).

Uncertainties in the climate effects of forest cover can complicate climate model simulations in heavily forested regions, such as the northeastern United States (US). For example, when global climate models were statistically downscaled over the northeastern US region, trends in observed winter warming (+0.7 °C/decade) were greatly underestimated by a CMIP3 model ensemble mean (+0.25 °C/decade) over the period 1970–2000 (Hayhoe et al., 2007). The underestimation of winter temperature trends in the downscaled models may be linked to poor parameterization of surface albedo over forests that contributes to the strength of snow albedo feedback (SAF) in the climate models (Hayhoe et al., 2007), which generally exhibit a three- to five-fold spread in the change in surface albedo associated with a 1 °C change in surface air temperature (Qu & Hall, 2006, 2014). Models with weaker SAF tend to have explicit canopy treatment and either have snow canopy albedos that are too low or have vegetation that excessively shields snow-covered surfaces, while models with stronger SAF generally have a greater contrast between snow-covered and snow-free conditions over forests (Qu & Hall, 2006, 2014).

Snow-covered reflectance and albedo products from satellite measurements have not been assessed for accuracy as extensively for forested landscapes (Wang et al., 2014) as they have for non-forested landscapes (e.g., Jin et al., 2003b; Klein & Stroeve, 2002; Stroeve, Box, & Haran, 2006; Stroeve, Box, Wang, Schaaf, & Barrett, 2013; Wang et al., 2012). Here, we focused on evaluating winter surface reflectance and albedo properties of landscapes in New Hampshire (NH), USA, a region dominated by second growth mixed temperate forest, interspersed with patches of agricultural and other human dominated land cover types. Landscape heterogeneity in the region complicates comparisons of ground-based and satellite albedo because the ground footprint of a tower based measurement may not be representative of the satellite footprint (Román et al., 2009; Wang et al., 2014). In such situations, an intermediate resolution product must be used to connect ground- and tower-based measurements to coarse resolution satellite imagery.

The MODerate resolution Imaging Spectroradiometer (MODIS) bidirectional reflectance distribution function (BRDF) albedo product (Schaaf, Liu, Gao, & Strahler, 2011; Schaaf et al., 2002; Schaaf et al., 2008) has been validated extensively over a variety of land cover types (Jin, Schaaf, Gao, Li, & Strahler, 2003a; Jin et al., 2003b; Liu et al., 2009; Salomon, Schaaf, Strahler, Gao, & Jin, 2006; Wang et al., 2012; Wright et al., 2014). The BRDF provides surface reflectance as a function of illumination and viewing geometry, and accounting for the unique structural and optical scattering, transmittance, absorption, and emission properties of a surface. Validation efforts have included shortwave broadband albedo (300–2800 nm) over the Greenland Ice Sheet (Stroeve et al., 2013), over snow-free (Román et al., 2009) and snow-covered forests (Wang et al., 2014), and spectral albedo over the Greenland Ice Sheet (Wright et al., 2014). These previous studies have demonstrated that MODIS BRDF albedo products perform very well over homogeneous landscapes. However, more research is needed to establish how well they perform over landscapes with high spatial heterogeneity. This is particularly important during periods of snow cover when highly reflective snow-covered fields stand in contrast to adjacent forested areas that mask snow cover with their dark canopies.

The daily MODIS snow albedo product (Hall, Salomonson, & Riggs, 2006) differs from the MODIS BRDF albedo product primarily in its assumption that forested lands are Lambertian reflectors (i.e., no BRDF correction is applied). The Lambertian assumption does not recognize the importance of forest clumping and canopy structure and does not account for shadows cast on adjoining foliage and in gaps in the forest canopy, which significantly alters the surface albedo. These geometric optical effects cause surfaces to appear darker when the source of illumination is opposite the MODIS viewing sensor (forward scattering) or brighter when the source of illumination is behind the sensor (backscattering), significantly impacting the retrieval of accurate snow-covered forest albedo. A higher BRDF could be expected in the viewing direction of forests with wider canopy gaps, where more underlying snowpack would be revealed. It is these shadowing effects that also drive the retention and melt of snow underlying canopy. Nonetheless, daily resolution makes the daily MODIS snow albedo product an ideal dataset for studying rapid changes in albedo as snow surfaces melt or compact. The daily MODIS snow albedo product has been validated over the Greenland Ice Sheet and shown to be biased low (−0.05) relative to ground-based measurements, though the variability in daily snow albedo is greater than that observed at ground-based stations (Stroeve et al., 2006). Daily MODIS snow albedo values were within 10% of ground-based observations collected during the 2004 ablation season in the complex terrain of Karasu Basin, Turkey (Tekeli, Şensoy, Şorman, Akyürek, & Şorman, 2006). A study comparing the MODIS daily snow albedo product to the 16-day MODIS BRDF albedo product over the Greenland Ice Sheet found good correspondence at lower elevations and poorer correspondence at higher elevations (Hall, Schaaf, Wang, & Riggs, 2009a). Hall, Nghiem, Schaaf, DiGirolamo, and Neumann (2009b) note that more work is needed to understand the limitations of daily snow albedo products. To the best of our knowledge, no comparison of the two products over forested and heterogeneous surfaces in the presence of snow-cover has been conducted.

In this study, ground- and tower-based estimates of albedo from surface reflectance quantities collected over snow-covered forest and open pasture were compared to HSI. After a spatial representativeness assessment, the HSI data were spatially aggregated to the resolution of MODIS pixels (~500 m) to assess the accuracy of MODIS BRDF and MODIS daily snow albedo products over heterogeneous landscapes including deciduous broadleaf, mixed forest, mixed forest/cropland/grassland mosaic, and urban & built-up land cover types. This study also examined the spectral albedo over a deciduous broadleaf forest canopy during snow-free dormant conditions and over a range of snow-cover depths using a tower-based field spectroradiometer to evaluate the extent of vegetation masking by forest canopies in the region.

2. Datasets

2.1. Study areas and ground instrumentation

The study focused on two research sites in New Hampshire, USA: (1) Thompson Farm Research Station (TF) in Durham, NH and (2) Bartlett Experimental Forest (BF) in Bartlett, NH (Fig. 1). Ground validation protocols are described in more detail below and summarized in Table 1. Details on the aircraft high resolution hyperspectral flight campaign carried out at the two research sites are provided in Section 2.2.

2.1.1. Thompson Farm (TF) Research Station

The TF Research Station is a 0.83 km^2 mixed use property that includes managed and unmanaged forests, freshwater marshes, and active agricultural fields (Fig. 2). The mixed deciduous and coniferous forest is composed primarily of northern red oak (*Quercus rubra*), white pine (*Pinus strobus*), red maple (*Acer rubrum*), shagbark hickory (*Carya ovata*), and white oak (*Quercus alba*) (Perron, Bennett, & Lee, 2004). The primary agricultural field located east of the canopy tower (Fig. 2) was tilled, manured, and replanted with pasture grass in late October 2012. The TF research station study area included two ground validation sites: (1) a pasture site (TFP) and (2) an above-canopy site (TFC).

At the TFP site, ground validation reflectance-based quantities included spectral radiance, spectral hemispherical conical reflectance factors (HCRF), shortwave broadband bihemispherical reflectance

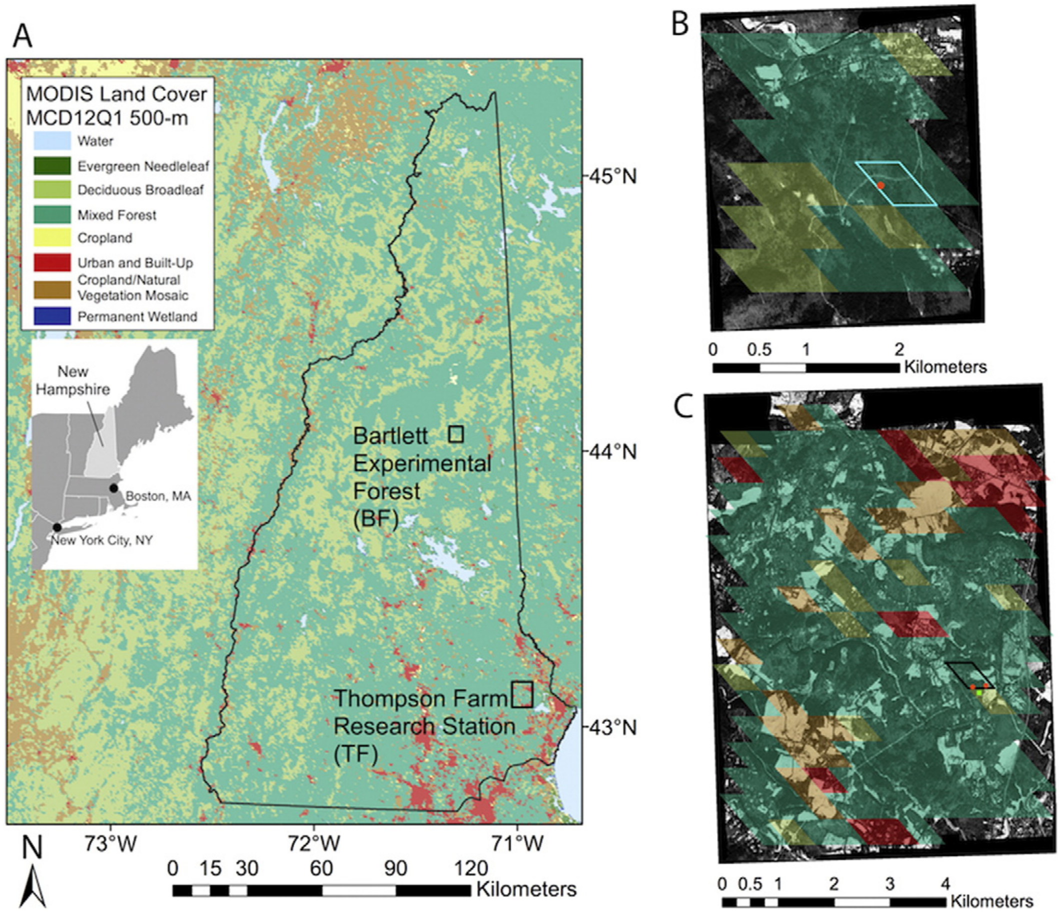

Fig. 1. (A) Hyperspectral flight study areas (boxes) and MODIS Combined Terra/Aqua 500-m (MCD12Q1) land cover in New Hampshire. Ground validation sites (orange dots) at (B) Bartlett Experimental Forest (BF) and (C) Thompson Farm Research Station (TF).

(hereafter, albedo; Schaepman-Strub, Schaepman, Painter, Dangel, & Martonchik, 2006) and spectral albedo (Table 1). Spectral surface radiance, HCRF, and albedo were collected using an Analytical Spectral Devices (ASD) FieldSpec4 (FS4) spectroradiometer with a nominal spectral resolution of 3 nm at 700 nm and 10 nm at 1400 nm and 2100 nm. Spectral measurements were collected every 0.9 m along a 46.6 m east–west transect at TFP (Fig. 2B, C). Snow depth generally increased east to west as one moved closer to the forest edge along the transect; total snow depth ranged from 8.0 cm to 26.0 cm with an average snow depth of 14.6 cm. Snow density was collected in a snow pit about 5 m north of a tower located in the middle of the transect using an aluminum snow tube and digital hanging scale (Table 1).

Table 1
Tower instrumentation, solar zenith angle (°) at the time of Analytical Spectral Devices (ASD) spectroradiometer measurements, timing of hyperspectral imagery (HSI) acquisition, and snow depth and density at research areas.

	Thompson Farm (TF)		Bartlett Experimental Forest (BF)
	TF-Pasture	TF-Canopy	
Tower latitude	43.1085 N	43.1085 N	44.0646 N
Tower longitude	−70.9486 W	−70.9522 W	−71.2881 W
Tower footprint diameter	18.9 m	379 m	316 m
Tower albedo[a] time	1600–1730 GMT	1600–1730 GMT	1600–1700 GMT
ASD solar zenith angles, SZA (°)			
ASD 25° FOV Radiance	48°–50°	–	–
ASD 25° FOV HCRF[b]	50°–51°	–	–
ASD Remote Cosine Receptor Albedo	48°–50°	48°	–
HSI Flight Avg. SZA (°)	48°	48°	50°
HSI flight time	1639–1702 GMT	1639–1702 GMT	1611–1621 GMT
Snow depth (cm)	8.0 cm–26.0 cm	25.4 cm	50 cm–100 cm[c]
Snow density (kg m^{-3})	340 kg m^{-3}	396 kg m^{-3}	200-300 kg m^{-3}[c]

[a] 30-minute average.
[b] Hemispherical conical reflectance factor.
[c] Estimated from NOHRSC-SNODAS.

Radiance and HCRF were collected at TFP using the bare fiber (25° FOV) over the surface of the snowpack relative to a calibrated Spectralon reference standard manufactured by LabSphere. Spectral albedo quantities were collected using the ASD with remote cosine receptor (RCR) foreoptic mounted to a 0.9 m leveling boom every 0.9 m along the same east–west transect; however, battery life of the ASD spectroradiometer limited the length of the spectral albedo transect to 35 m. Five RCR albedo spectra were collected at each location along the 35 m transect, calculated as the ratio of incoming irradiance and outgoing irradiance. Shortwave (280–2800 nm) broadband albedo (30-min averaged) was collected using a Kipp and Zonen CMA6 albedometer (half field of view = 81°; Michalsky, Harrison, & Berheiser, 1995) mounted 1.5 m above the snowpack in the middle of the 46.6 m transect. The tower footprint diameter, *f*, is calculated using the following equation:

$$f = 2h\tan(HFOV^{\circ}) \quad (1)$$

where *h* is the height of the instrument mounted to the tower (30 m) and *HFOV*° is the half field of view.

At the Thompson Farm Canopy (TFC) site (Fig. 2), tower validation included collection of shortwave broadband albedo and spectral albedo above the forest canopy from a 30-m tower. A Kipp and Zonen CMA6

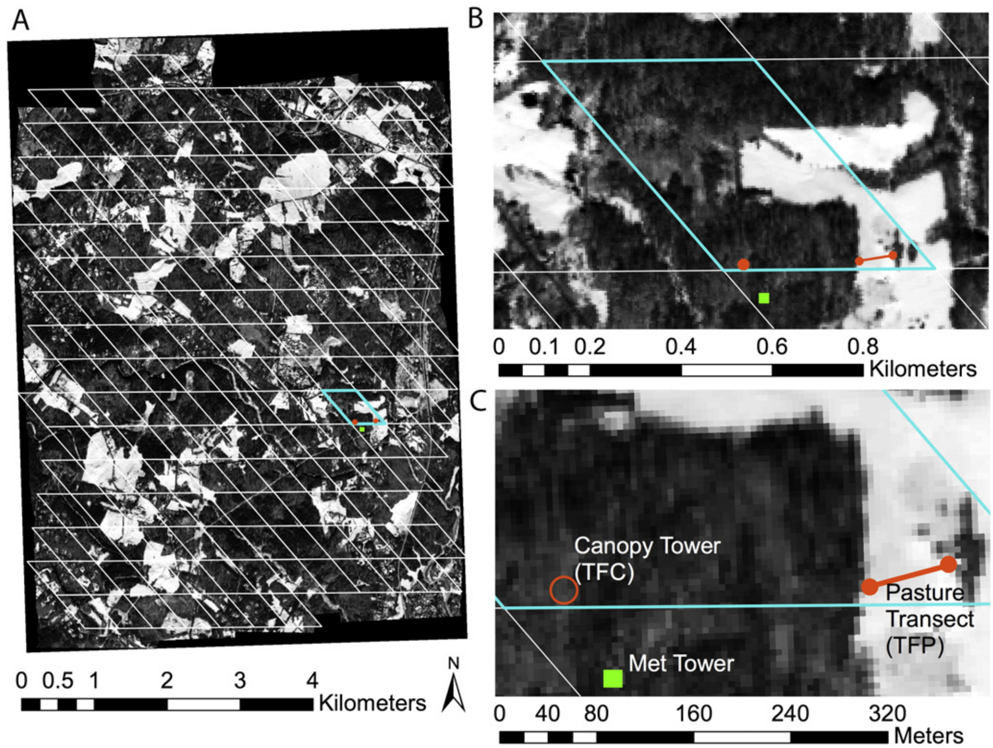

Fig. 2. (A) Thompson Farm hyperspectral flight study area in southeastern New Hampshire with MODIS pixel boundaries (white). (B) Inset shows location of TFC above-canopy tower validation site, TFC Meteorological/AERONET (Met) tower, and TFP ground validation transect site. (C) Closer view of TFP transect and proximity to TFC tower and Meteorological/AERONET tower.

albedometer collected 30-min averaged shortwave broadband albedo over the spectral range 280–2800 nm. The CMA6 albedometer was mounted at the end of a 4.5-m long horizontal leveling boom positioned approximately 5 m above a red oak (*Q. rubra*) dominated portion of the mixed forest. No canopy snow was present during the measurements. Snow depth and snow density were collected in a snow pit about 20 m north of the tower using an aluminum snow tube and digital hanging scale (Table 1).

Spectral albedo over the forest canopy was measured using the ASD FS4 spectroradiometer. It was not practical to collect radiance or spectral reflectance from the tower. Albedo spectra were collected using the manufacturer's remote cosine receptor (RCR) foreoptic (~81° HFOV) attached to a 4.5 m long leveling boom protruding southward 5 m above the same red oak (*Q. rubra*) dominated portion of the mixed forest as the Kipp and Zonen CM6 albedometer. Spectral albedo above the canopy was calculated as the ratio of upwelling to downwelling irradiance. A total of ten albedo spectra were collected between 1623 GMT and 1632 GMT on 2013-03-09, less than 10 min prior to the hyperspectral overflight transect at 1639 GMT (Table 1).

TFC spectral albedo and CMA6 broadband albedo were also collected using the ASD FS4 with RCR foreoptic from the same tower location during snow-free dormant conditions on 2012-03-19 and over snow depths ranging from 6.4 cm to 39.4 cm between 2012-03-08 and 2013-03-09 and snow densities ranging from 178 kg m^{-3} to 448 kg m^{-3} (Table 2). No canopy snow was present during any of the measurements. HSI data were only available for 2013-03-09.

2.1.2. Bartlett Experimental Forest, Bartlett, NH (BF)

The Bartlett Experimental Forest (BF) was established as an experimental forest by the United States Department of Agriculture Forest Service (USDA-FS) in 1932 and includes 10.52 km^2 of mixed northern deciduous and coniferous species (Fig. 3). Common deciduous species include American beech (*Fagus grandifolia* Ehrh.), red maple (*A. rubrum* L.), sugar maple (*Acer saccharum* Marsh.), and yellow birch (*Betula alleghaniensis* Britton). Coniferous species include red spruce (*Picea rubens* Sarg.), balsam fir (*Abies balsamea* (L.) Mill.), and eastern hemlock (*Tsuga canadensis* (L.) Carrièr). The silviculture history is well documented and includes a recent patch harvest southwest of the tower within the HSI sampling domain (Fig. 3).

Tower-based instrumentation at BF included two Kipp and Zonen CM3 pyranometers (spectral range 280–2800 nm) that collected 30-minute averaged values of incoming (upward facing unit) and reflected (downward facing unit) solar radiation (Table 1). The CM3 pyranometers were mounted at a height of 25 m on a 30 m tower, approximately 8 m above a beech and maple-dominated portion of the forest canopy (Fig. 3C). No data were collected with the ASD spectroradiometer at BF.

2.2. Hyperspectral imagery (HSI) acquisition

High resolution hyperspectral imagery (HSI) was acquired using the ProSpecTIR VNIR/SWIR 4 (VS4) sensor on 2013-03-09 (Table 1). The ProSpecTIR VS4 sensor collected calibrated radiance data (mW/cm^2/µm/sr) from raw imagery over the spectral range 400 nm to 2450 nm at nominal spectral resolution of 5 nm in 360 bands. The ProSpecTIR VS4 was flown at an average altitude of 4125 m with an instantaneous field of view of 0.029°, yielding a spatial resolution of 5 m and swath width of 1700 m with 35% sidelap between flight lines.

Table 2
Above-canopy spectral albedo measurements collected using the ASD with RCR foreoptic at Thompson Farm Canopy (TFC) between 2012-03-08 and 2013-03-09.

Date	Clouds	Solar zenith angle (°)	CMA6 broadband albedo	Snow depth (cm)	Snow density (kg m^{-3})
2012-03-08	Clear	49°	0.15	6.4	285
2012-03-19	Clear	47°	0.10	0	–
2013-01-15	Partly cloudy	65°	0.18	12.7	448
2013-02-10	Clear	57°	0.14	39.4	178
2013-03-09	Clear	48°	0.14	25.4	396

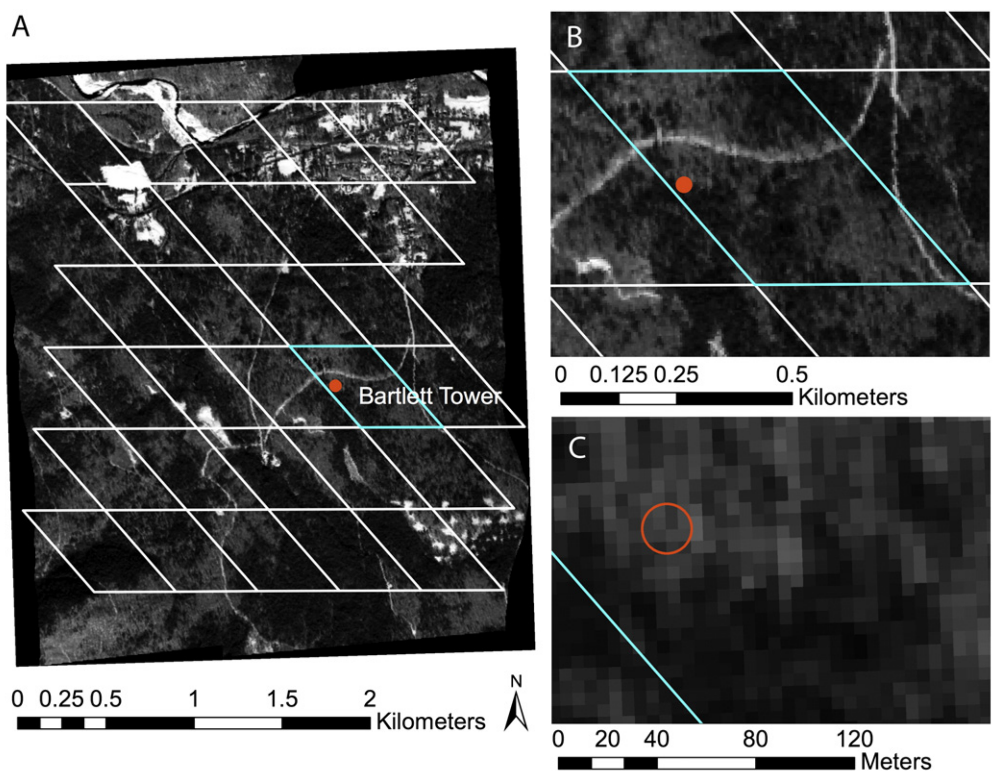

Fig. 3. (A) Bartlett Experimental Forest (BF) hyperspectral flight study area in northern New Hampshire with MODIS pixel boundaries (white) and above-canopy tower location (orange circle). (B) Tower location and proximity to access road, and (C) closeup of tower location.

The flight campaign was conducted less than 12 hours after a snowfall event on 2013-03-08. The event deposited new snowfall atop an existing snowpack across the state of New Hampshire, with a new snowfall total of 7.62 cm measured at the Thompson Farm pasture tower site. Snowfall totals from the 2013-03-08 storm were not recorded at BF. Total snowpack depth (~50–75 cm) at BF was estimated from the National Operational Hydrologic Remote Sensing Center (NOHRSC) daily 1-km snow depth product (National Operational Hydrologic Remote Sensing Center (NOHRSC), 2004) (Table 1).

The MODerate resolution atmospheric TRANsmission (MODTRAN4) model was used in conjunction with the ATmospheric CORrection (ATCOR4) software package to convert ProSpecTIR VS radiance data into reflectance using the following algorithm,

$$\rho = \frac{\pi\left\{d^2(L_s)-L_{path}\right\}}{\tau E_g}$$

where τ is the atmospheric transmittance, L_s is the calibrated sensor radiance, L_{path} is the path radiance, or photons scattered into the sensor's instantaneous field of view without having ground contact, E_g is the downwelling irradiance on the ground, and d is the sun-to-Earth distance in astronomical units. Downwelling irradiance was derived from the pre-calculated MODTRAN4 database. Radiance and reflectance imagery were georeferenced using SpecTIR's Inertial Navigation Systems (INS) in conjunction with the United States Geological Survey National Elevation Dataset Digital Elevation Model at 10 m resolution and Geographic Lookup Tables (GLT). To calculate τ, SpecTIR's application of the ATCOR4 program assumed a rural aerosol type (aerosol optical depth = 0.092), 100 km visibility, 1% cloud cover based on flight logs, and water vapor content derived from absorption features in the HSI data at 1130 nm.

2.3. MODerate Resolution Imaging Spectroradiometer (MODIS) data

We assessed the accuracy of two MODIS products: (1) MCD43 V005 (which combines data from both Terra and Aqua platforms) and (2) the MOD10A1 V005 (Terra only) daily shortwave broadband albedo product. Both MCD43 and MOD10A1 use the Normalized Difference Snow Index (NDSI) to detect snow cover for a MODIS pixel (Eq. (3)):

$$\text{NDSI} = \frac{\text{Band 4}-\text{Band 6}}{\text{Band 4}+\text{Band 6}}. \tag{2}$$

The NDSI exploits the high reflectance of snow in the visible part of the spectrum using Band 4 (545–565 nm) and strong absorption in the near-infrared using Band 6 (1628–1652 nm). Due to a failure of Band 6 shortly after launch, MODIS/Aqua NDSI substitutes Band 6 with Band 7 (2105–2155 nm) reflectance (Hall & Riggs, 2007). For non-forested landscapes, a pixel is classified as snow when the NDSI is greater than 0.4. The low reflectance of forest canopies necessitates using the NDSI in conjunction with the normalized difference vegetation index (NDVI) to detect snow cover under the canopy (Klein, Hall, & Riggs, 1998):

$$\text{NDVI} = \frac{\text{Band 1}-\text{Band 2}}{\text{Band 1}+\text{Band 2}}. \tag{3}$$

Use of the NDVI exploits the increase in the visible using Band 1 (620–670 nm) with respect to reflectance in the NIR using Band 2 (841–876 nm). Forested areas are classified as snow-covered if the NDSI is between 0.1 and 0.4 and if the NDVI is ~0.1 (Klein et al., 1998; Riggs, Hall, & Salomonson, 2006).

2.3.1. MCD43 BRDF/Albedo product

Within the MCD43 V005 product suite, we evaluated the MCD43A4 Nadir BRDF-Adjusted Reflectance (NBAR) product and the MCD43A3 standard BRDF/Albedo product (Schaaf et al., 2002, 2011). The semi-empirical linear kernel-driven BRDF model characterizes the anisotropy of the surface, accounting for optical geometry, volumetric scattering, view angle, and solar zenith angle and is used to produce BRDF parameter weights for a full model inversion (high quality), given that at least seven cloud-free observations are available to adequately sample the angular anisotropy during a 16-day period. If a BRDF model cannot be fit to the data, or the data available are too few or inappropriate to capture the angular variation, a single day observation (in this case 2013-03-09) is used for a magnitude inversion with the a priori back-up algorithm information updated from the latest full model inversion and the BRDF parameters. Magnitude inversion MCD43A3 BRDF/Albedo data are assigned a poor quality flag.

The MCD43A4 NBAR product is computed for MODIS spectral bands 1–7 (Table 3) at local solar noon for a given 16-day period. The computation removes view angle effects from directional reflectances, resulting in a more stable and consistent product for comparison with ground- and tower-based observations.

The BRDF/Albedo (MCD43A3) product includes bihemispherical reflectance (white-sky albedo) and directional–hemispherical reflectance (black-sky albedo) at local solar noon as spectral and shortwave broadband quantities at 500-m sinusoidal gridded resolution (Schaaf et al., 2002; Schaaf et al., 2011). The linear combination of diffuse and direct components, known as blue-sky albedo ($A_{\Lambda iso}$), at a given solar geometry (Ω_s), can be calculated based on the proportion of diffuse illumination for a totally absorbing lower boundary ($D_{0\Lambda}$) using the following equation (Román et al., 2010):

$$A_{\Lambda iso} = f_{iso\Lambda} + (1 - D_{0\Lambda})\left[f_{vol\Lambda}\overline{K}_{vol}(\Omega_s) + f_{geo\Lambda}\overline{K}_{geo}(\Omega_s)\right] + D_{0\Lambda}\left[f_{vol\Lambda}\overline{K}_{vol}(\Omega_s) + f_{geo\Lambda}\overline{K}_{geo}(\Omega_s)\right] \quad (4)$$

where Λ is a MODIS waveband (Table 3), D_0 is the proportion of diffuse illumination for a totally absorbing lower boundary, $\overline{K}$ is the directional-hemispherical integral, $f_{x\Lambda}$ is the RossThick–LiSparse Reciprocal Bidirectional Reflectance Factor (BRF), and the subscript x indicates isotropic (*iso*) scattering, geometric-optic (*geo*) surface scattering, and volumetric (*vol*) scattering.

Narrowband (α_i; Table 3) MCD43A3 blue-sky albedo data were converted to shortwave broadband albedo (α_{sw}) for snow-covered surfaces after Stroeve et al. (2005):

$$a_{sw} = 0.1574\alpha_1 + 0.2789\alpha_2 + 0.3829\alpha_3 + 0.1131\alpha_5 + 0.0694\alpha_7 - 0.0093. \quad (5)$$

High quality (full inversion) MCD43A3 albedo data were not available for the 16-day period surrounding 2013-03-09. Instead, a local magnitude inversion was run for the TF and BF HSI study areas, with a modeling assumption of completely clear skies (e.g., little to no scattering from cloud and aerosol) and using only MODIS retrievals for 2013-03-09. The assumption of clear atmospheric conditions was supported by ground-based observations by the ground validation team, clear skies identified in Aqua reflectance imagery, and aerosol optical thickness of 0.05 measured at the Thompson Farm Research Station by the AERONET Cimel Spectral Radiometer (sun photometer). Clear sky data from 2013-03-10 were not included in the BRDF model because of extensive snow melt observed in the Thompson Farm Study Area. The locally run Collection V005 MCD43 magnitude inversion was flagged as a poor quality BRDF/Albedo product for 2013-03-09.

Table 3
MODIS bands used in this study.

MODIS band	Spectral range (nm)
1	620–670
2	841–876
3	459–479
4	545–565
5	1230–1250
6	1628–1652
7	2105–2155

2.3.2. MOD10A1 daily snow-covered albedo

The MODIS/Terra Snow Cover Daily L3 global 500 m gridded product (MOD10A1) was retrieved from the National Snow and Ice Data Center (NSIDC) (Hall et al., 2006). MOD10A1 daily shortwave broadband albedo is produced for cloud-free, snow-covered pixels using the atmospherically corrected MODIS/Terra surface reflectance product (MOD09GHK) and uses bidirectional reflectance distribution function (BRDF) look up tables to correct for surface anisotropy based on solar zenith angle, sensor zenith, relative azimuth at the time of Terra overpass together with surface slope, aspect and MCD12Q1 land cover type (see Klein and Stroeve (2002) for more detail on the MOD10A1 algorithm). In MOD10A1, albedo estimates for snow-covered pixels in non-forested areas are adjusted for anisotropic scattering effects using the DIScrete Ordinates Radiative Transfer (DISORT) model and snow optical properties (Klein & Stroeve, 2002); forested land cover types identified in MCD12Q1 are assumed to be Lambertian reflectors in MOD10A1 and no BRDF corrections are applied.

2.3.3. MCD12Q1 land cover

The MODIS Terra/Aqua Combined Annual L3 Global 500-m land cover dataset (MCD12Q1) is created using a supervised classification methodology described in more detail in Friedl et al. (2002, 2010). Our analysis used the International Geosphere–Biosphere Programme (IGBP) classification scheme, and included deciduous broadleaf, mixed forest, cropland/natural mosaic, and urban & built-up land cover classes in the two study areas (Fig. 1). Cropland/natural mosaic is defined as “lands with a mosaic of croplands, forests, shrubland, and grasslands in which no one component comprises more than 60% of the landscape” (Friedl et al., 2002).

2.4. Landsat 5 data

Landsat 5 Thematic Mapper (TM) data at 30-m spatial resolution were retrieved from the United States Geological Survey (USGS) and used to assess spatial representativeness of the TF and BF research areas in the presence of snow cover. Top of the atmosphere spectral reflectances were derived from radiometric calibration of Level 1 Digital Number (DN) using solar irradiance tables with the view and illumination conditions at the time of satellite overpass. Directional surface reflectance was then produced using atmospheric corrections provided by the Second Simulation of the Satellite Signal in the Solar Spectrum (6S) radiative transfer code (Kotchenova, Vermote, Matarrese, & Klemm, 2006; Vermote et al., 1997). Shortwave reflectance (r_{sw}) was calculated using narrowband (r_i) to broadband coefficients specific to Landsat data (Liang, 2001):

$$r_{sw} = 0.356r_1 + 0.130r_3 + 0.373r_4 + 0.085r_5 + 0.072r_7 - 0.0018. \quad (6)$$

The shortwave reflectance is then converted to albedo using an Anisotropic Reflectance Factor (ARF) taken from the nearest available pure high quality MODIS pixel adjacent to the tower site and comprised of the same land cover class (Shuai, Masek, Gao, & Schaaf, 2011).

3. Methods

3.1. Spatial representativeness metrics

Because the tower footprint diameters for TFP (18.9 m), TFC (379 m), and BF (315 m) are substantially smaller than the size of a 500-m MODIS pixel, we used a variogram model (Carroll & Cressie,

1996) to assess the spatial representativeness of the TFC and BF measurement footprints relative to the MODIS measurement footprint. The range (a), sill (c), and nugget effect (c_o) are the spatial attributes modified to fit a spherical model to the variogram estimator (for more detailed description of the variogram model, see Román et al., 2009; Román et al., 2010; Wang et al., 2014).

The range (a) describes the average patch size of the landscape at which there is no further correlation of biophysical property associated with the point of interest (e.g., the tower location). In the case where the satellite footprint is larger than the measurement footprint, the range value of a spatially representative site should be equal to or less than that of the satellite.

The sill (c) describes the maximum semivariance (or maximum overall variation) and is the value of the range at which the variogram levels to an asymptote (Fig. 4). A smaller sill value is indicative of a more homogeneous surface for which ground measurements are more spatially representative. Larger sill values point toward more heterogeneous landscape structure.

The nugget effect (c_o) describes the value at which the variogram does not reach zero variance at a lag distance $h = 0$ and depends on the variance associated with small-scale variability, measurement errors, or a combination of both (Noreus, Nyborg, & Hayling, 1997). The nugget effect is indicative of pure random variation.

In addition to the sill, range, and nugget effect, several geostatistical attributes of spatial representativeness are derived from the semivariogram model (Román et al., 2009). These include the relative coefficient of variation (R_{CV}), the scale requirement index (R_{SE}), the relative proportion of structural variation (R_{SV}), and the relative strength of spatial correlation (R_{ST}) (for detailed description of these attributes; see Román et al., 2009).

For R_{CV}, a spatially representative site should have a value that approaches zero because the overall variability between the components internal to the ground measurement site should be similar in magnitude to the external landscape included in the satellite footprint. A large positive value is indicative of greater variability in the landscape external to the assessed spatial scale (here 0.3 km, a proxy for the tower footprint) while a negative value is indicative of greater variability within the assessed scale (Román et al., 2009).

The R_{SE} examines the variogram range of two spatial extents with respect to the tower instrument field of view. Spatially representative ground measurement sites should have R_{SE} values between 0 and $\approx$0.243%.

The R_{SV} is a function of the range (a), nugget (c_o), sill (c), and variogram estimator and accounts for the relative change in structural variation with increasing field of view. Large positive values for R_{SV} occur when landscape patchiness increases from the assessed scale (0.3 km) to the reference scale (here, 1.0 km). Large negative values indicate that patchiness of the extended footprint is less than the patchiness within the assessed subset footprint.

The R_{ST} provides an indicator for whether outliers lie within the small subset footprint or are external to the smallest subset footprint. Negative R_{ST} values indicate outliers are more commonly occurring within the small subset while positive R_{ST} values are attributed to outliers external to the smallest subset.

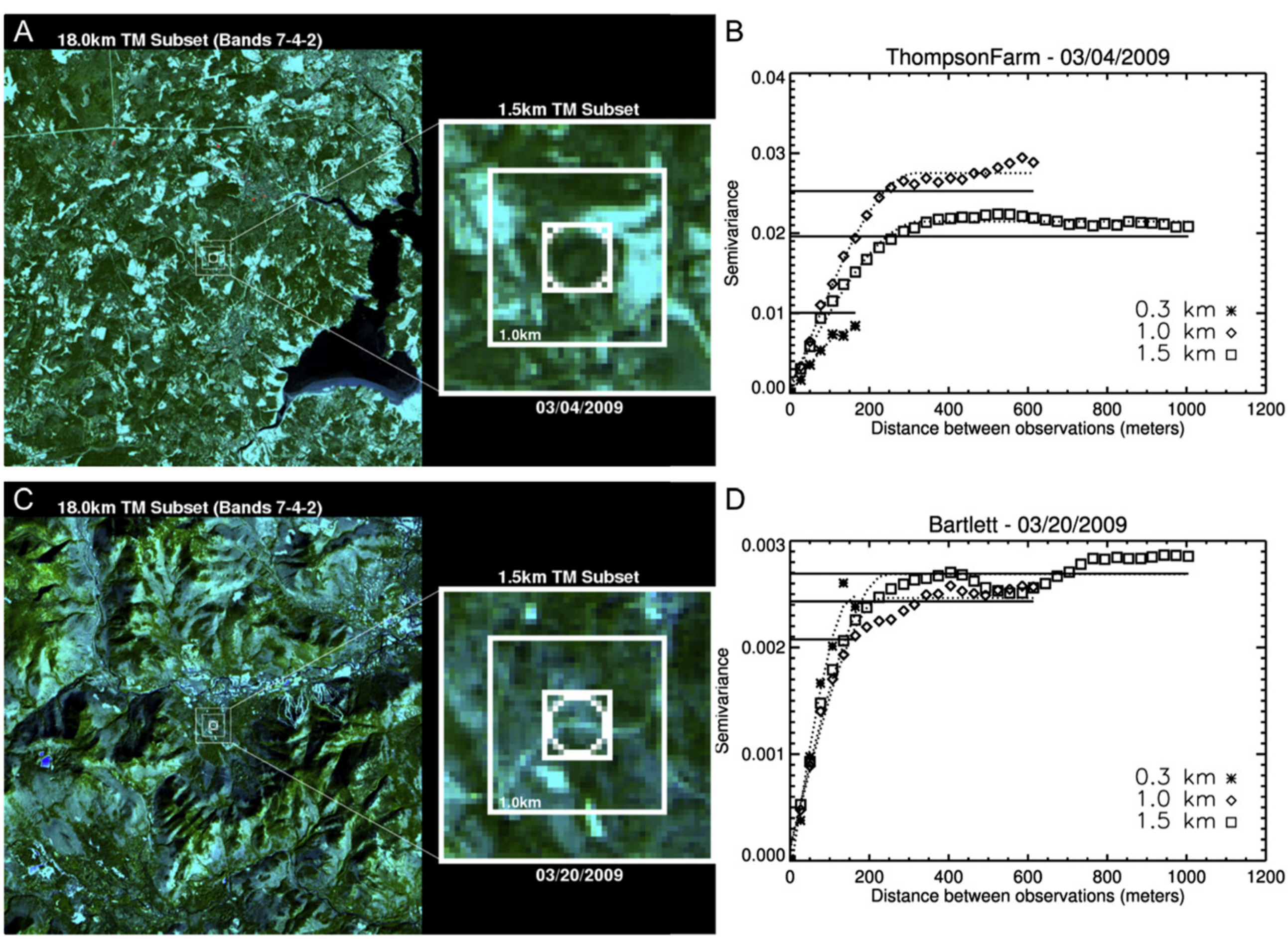

Fig. 4. Top-of-Atmosphere shortwave reflectance composite of Landsat 5 TM (bands 7, 4, and 2) and semivariogram function, variogram estimator (points), spherical model (dotted curve), and sample variance (solid straight lines) using 0.3 km (asterisks), 1.0 km (diamonds), and 1.5 km (squares) satellite subsets centered over the (A) Thompson Farm Canopy (TFC) tower site and (B) Bartlett Experimental Forest (BF) tower site.

3.2. Ground and tower HSI comparison protocols

3.2.1. Spectral radiance, HCRF, and albedo

Ground- and tower-based spectral radiance, HCRF, and albedo were compared to HSI radiance and reflectance spatially subsetted from the HSI imagery for the TFC and BF tower footprints and for the TFP transect. Above the canopy at TFC, spectral albedo measurements were collected using the ASD/RCR; no radiance or HCRF data were collected. TFC spectral albedo tower measurements were compared to HSI spectral reflectance.

3.2.2. Shortwave broadband albedo

Shortwave broadband albedo at the TFC and TFP tower sites was calculated as the sum of 30-minute averaged incoming values divided by the sum of 30-minute averaged reflected values collected between 1600 and 1730 GMT. The CM3 pyranometer data collected from the BF flux tower were retrieved through the AmeriFlux network website (http://public.ornl.gov/ameriflux/). Shortwave broadband albedo at BF was calculated as the sum of 30-minute averaged incoming values divided by the sum of 30-minute averaged reflected values collected between 1530 and 1630 GMT.

Shortwave broadband albedo was estimated from HSI surface reflectance by multiplying the 360 HSI reflectance bands by downwelling spectral irradiance and dividing the product by total irradiance 400 nm to 2450 nm. Downwelling irradiance spectra were modeled using Simple Model for Atmospheric Radiative Transfer of Sunshine (SMARTS v2.9.5; Gueymard, 1995; 2001). Irradiance simulations used atmospheric pressure data from the above-canopy meteorological station and aerosol optical depth (0.05) from the Aerosol RObotic NETwork (AERONET; http://aeronet.gsfc.nasa.gov/) station. The meteorological station and the AERONET station are located at the top of a walk-up tower above the forest canopy at Thompson Farm located about 40-m southeast of the TFC tower where above-canopy albedo was measured (Fig. 2C). The resultant HSI shortwave broadband albedo imagery was spatially subsetted for the TFP tower footprint, the TFC tower footprint and the BF tower footprint.

3.3. HSI and MODIS comparison protocols

3.3.1. HSI and MCD43A4 NBAR

HSI reflectance comparisons to MCD43A4 were limited to the Thompson Farm Study Area because the timing of overflight was the only acquisition close enough to local solar noon (1651 GMT), minimizing the effects of solar illumination geometry in the comparison. During image acquisition, the roll of the aircraft ranged from −1.511° and 2.333° and the pitch ranged from 0.136° to 1.330°. Therefore no BRDF-adjustments were attempted with the HSI reflectance data.

HSI reflectance imagery and MCD43A4 NBAR data were re-projected to a common datum (World Geodetic System (WGS) 1984 Universal Transverse Mercator (UTM), Zone 19 N) and zonal statistics (mean, standard deviation) were reported from the 5 m HSI pixels that fell within the boundaries of the 183 MCD43A4 ~500 m grid cells over the Thompson Farm Study Area.

3.3.2. HSI and MODIS shortwave broadband albedo

HSI, MCD43A3, and MOD10A1 shortwave broadband albedo were re-projected to a common datum and projection (WGS 1984 UTM 19 N) and zonal statistics were reported from the 5 m HSI pixels that fell within the ~500 m MODIS grid cells for the TF and BF study areas. Zonal statistics were also reported for the four MCD12Q1 IGBP land cover classes available: (1) deciduous broadleaf (TF and BF), (2) mixed forest (TF and BF), (3) urban and built-up (TF only), and (4) cropland natural/mosaic (TF only).

4. Results and discussion

4.1. Spatial representativeness

4.1.1. Spatial representativeness of TF study area

The TFC tower site was analyzed for spatial representativeness compared to the MODIS fields of view by averaging the 30 m Landsat TM data to 0.3 km, 1.0 km, and 1.5 km fields of view. In this analysis, the 0.3 km subset serves as a proxy for the TFC tower footprint and 1.0 km subset encompasses the variation attributable to the MODIS 0.5 km grid cell. While the MODIS retrievals were provided on a 0.5 km grid, the use of multiple multi-angle inputs result in values that are generally considered more applicable to an 800 m region (Wolfe et al., 2002). As the TFC and TFP tower sites are in close proximity to each other and located within the same gridded 500 m MODIS pixel (Fig. 2); spatial representativeness of both tower sites is assumed to be similar.

The TFC tower site is located in a mixed forest and the northeastern extent of the tower footprint captures the edge of the snow-covered pasture (Fig. 4A). Based on Landsat imagery acquired 04-Mar-2009, sill (c) values at TFC are relatively large, ranging from 0.00831 at 0.3 km, 0.02261 at 1.0 km, and 0.02042 at 1.5 km (Fig. 4A; Table 4). The range (a) is 164.09 m for the 0.3 km statistical area, increasing to 314.94 m at 1.0 km and to 328.52 m at 1.5 km. When the Landsat 5 TM footprint was increased from 0.3 km to 1.0 km, the relative coefficient of variation (R_{CV}) increased by 10.61%, the relative strength of spatial correlation (R_{ST}) increased by 62.99%, the relative proportion of structural variation (R_{SV}) increased 71.61%, and the relative scale requirement index (R_{SE}) increased by 7.40% (Table 4). The maximum semi-variance (sill) values at Thompson Farm were greater than 0.001, indicative of a spatially heterogeneous tower site (Fig. 4A; Table 4). The high spatial heterogeneity of all subsets, based on the large snow patches visible in the pasture, suggest that direct assessment between the tower footprint and MODIS albedo is not suitable for the Thompson Farm Canopy tower site during periods of snow cover. Use of intermediate resolution (e.g., HSI) data is necessary for comparison of ground-based measurements to MODIS.

4.1.2. Spatial representativeness of BF study area

During periods of snow-cover, the access road that runs through the BF tower footprint is clearly visible (Fig. 4B). Snow can be seen through the canopy to varying degrees throughout the Landsat scene, likely dependent on stand density and tree species. Two recently harvested areas located south of the tower footprint can also be detected by their brighter snow cover within the 1.0 km area.

At BF, sill (c) values span from .002617 at 0.3 km, 0.002362 at 1.0 km, and 0.002564 at 1.5 km (Fig. 4B; Table 4). At BF, geostatistical attributes

Table 4
Geostatistical attributes of spatial representativeness at Thompson Farm Canopy (TFC) and Bartlett Experimental Forest (BF) tower sites.

	TFC	BF
Landsat 5 acquisition date	04-Mar-2009	20-Mar-2009
Ground conditions	Snow-covered	Snow-covered
Tower footprint	379 m	315 m
$Range_{0.3\ km}$	164.09 m	160.21 m
$Range_{1.0\ km}$	314.94 m	232.36 m
$Range_{1.5\ km}$	328.52 m	244.3 m
R_{CV}	10.61%	18.52%
R_{SE}	7.40%	9.132%
R_{ST}	62.99%	30.94%
R_{SV}	71.61%	21.94%
$Sill_{0.3\ km}$	0.00831	0.002617
$Sill_{1.0\ km}$	0.02729	0.002362
$Sill_{1.5\ km}$	0.02042	0.002564

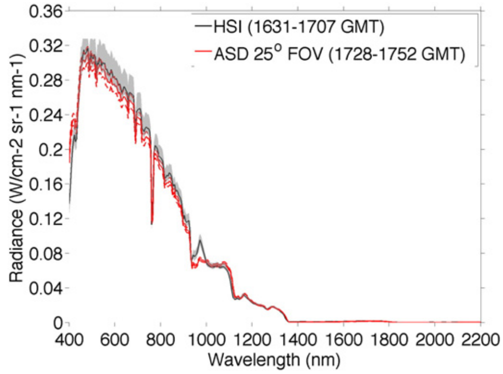

Fig. 5. ASD spectroradiometer radiance (red) and HSI (black line) radiance (W/cm^{-2} sr^{-1} nm^{-1}) collected on 2013-03-09 along the TFP transect. Timing of data collection is indicated in parentheses. Gray shading indicates range in HSI radiance values along the 46.6-m transect. Dashed red lines indicate 95% confidence intervals of ASD spectroradiometer samples along transect.

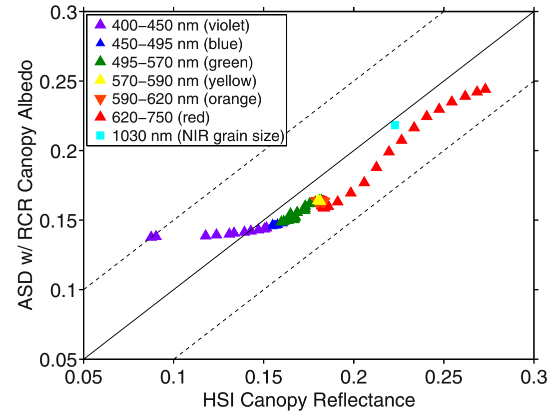

Fig. 7. HSI canopy reflectance vs. ASD with RCR foreoptic canopy albedo at Thompson Farm Canopy (TFC) shown for the visible wavelengths (colored triangles) and 1030 nm NIR wavelength (cyan square). Dashed lines represent ±0.05 absolute accuracy requirement recommended by Henderson-Sellers and Wilson (1983).

R_{ST} (30.938%), and R_{SV} (21.940%) were lower than respective values at the TFC tower site while R_{SE} (9.13%) and R_{CV} (18.52%) were greater than at TFC (Table 4). As with TFC, the high maximum semi-variance values are indicative of a spatially heterogeneous landscape in the presence of snow. Unlike TFC, however, the semi-variance values at BF do not increase dramatically with spatial scale. The spatial heterogeneity was most likely influenced by patch harvests to the south of the tower, the access road within the tower footprint, and the variable stand density and species distribution within and outside of the ~0.3 km tower footprint. Given the detected high spatial heterogeneity at the BF tower site in winter, use of intermediate resolution (e.g., HSI) data is warranted to facilitate comparison of ground-based measurements to MODIS footprints during periods of snow cover.

4.2. Ground- and tower-based HSI comparison

4.2.1. ASD spectrometer and HSI radiance

At TFP, mean spatially averaged 5 m HSI radiance (W/cm^{-2} sr^{-1} nm^{-1}) within the TFP transect footprint compared well to ground-based radiance collected with the ASD spectroradiometer and 25° FOV bare fiber (Fig. 5). Mean HSI radiance fell within the ASD radiance 95% confidence intervals throughout most of the Visible/Near Infrared (VNIR) and Shortwave Infrared (SWIR). The upper range in HSI radiance at TFP was greater than the ASD radiance 95% confidence intervals in the VNIR.

4.2.2. ASD spectrometer and HSI HCRF and albedo

Ground-based HCRF collected using the 25° FOV bare fiber along the 46.6-m transect at TFP were compared to MODTRAN-processed 5 m HSI reflectance pixels spatially averaged within the transect footprint. The steep decline in HSI reflectance below 450 nm (Fig. 6a) was not observed in the ground-based ASD 25° FOV HCRF or in the ASD with RCR foreoptic spectral albedo measurements. The underestimation of HSI reflectance in the visible part of the spectrum at TFP could be an atmospheric artifact caused by scattering of light by aerosols and water vapor located between the sensor mounted on the plane and the target

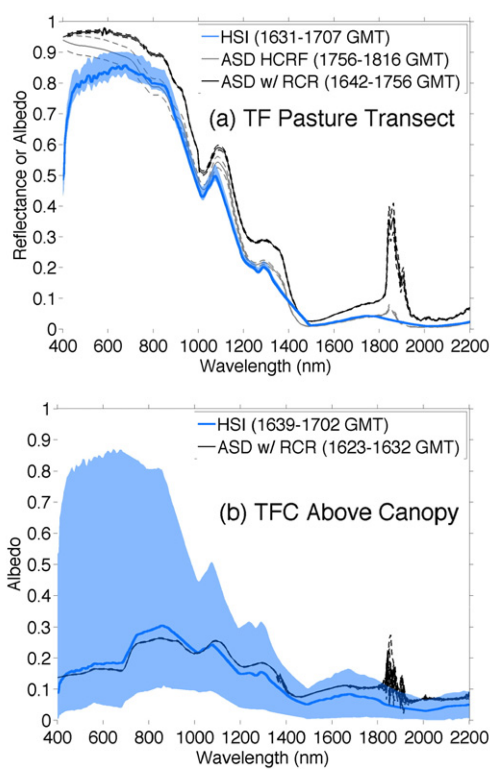

Fig. 6. Average HSI reflectance within tower footprint (blue line), ASD with 25° FOV bare fiber (gray) reflectance, and ASD with RCR foreoptic (black) albedo collected on 2013-03-09 at (a) TFP transect and (b) TFC. Blue shaded region represents the range of HSI pixel values collocated along the transect or within the tower footprint. Dashed lines show the 95% confidence intervals.

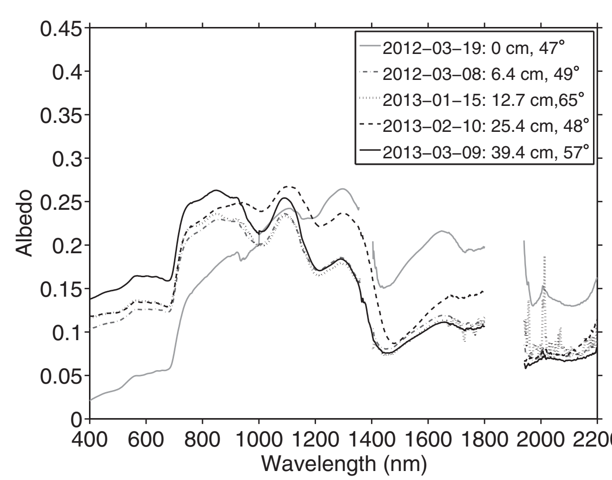

Fig. 8. Spectral albedo measured using the ASD FieldSpec4 and RCR (180° FOV) foreoptic above a dormant deciduous broadleaf canopy under a range of snow depths (cm) and solar zenith angles (°).

Table 5
Shortwave broadband albedo from tower-based ground validation sites and HSI pixels collocated with the tower footprints.

Site	Land cover	Snow depth (cm)	Tower-based albedo	HSI 2013-03-09	
				Albedo	SZA[b]
TFP	Dead pasture grass	11.0	0.71	0.67	48°
TFC	Dormant decid. broadleaf	25.4	0.17	0.19	48°
BF	Dormant decid. broadleaf	50–75[a]	0.19	0.18	50°

[a] Estimated from Snow Data Assimilation (SNODAS) data product (NOHRSC, 2004).
[b] Solar zenith angle.

on the ground (Vermote, El Saleous, & Justice, 2002). Given the strong correspondence between HSI radiance and ASD spectroradiometer radiance (Section 4.2.1), we suspect that overcorrection for atmospheric scattering during the processing of radiance to surface reflectance contributed to the steep decline in HSI reflectance relative to surface-based ASD spectroradiometer measurements.

Above the canopy at TFC, the mean spatially averaged 5 m HSI spectral albedo fell within ±0.05 compared to tower footprint ASD with RCR foreoptic albedo throughout visible and NIR wavelengths, though the range in HSI visible albedo was much greater than the ASD tower-based spectral albedo (Fig. 6b). The largest differences between HSI albedo and ASD with RCR foreoptic spectral albedo occurred at wavelengths below 450 nm but fell within ±0.05 (Fig. 7). The ASD with RCR foreoptic spectral albedo trended higher at wavelengths less than 700 nm. NIR reflectance at 1030 nm, indicative of an ice absorption feature related to optical grain size (Warren, 1982), fell within ±0.05, the absolute accuracy requirement for albedo recommended for use in climate modeling studies (Henderson-Sellers & Wilson, 1983).

Above-canopy spectra collected using the ASD with RCR foreoptic between 2012-03-08 and 2013-03-09 showed an increase of 0.1–0.2 in the visible part of the spectrum when snow was present under the bare canopy compared to snow-free, bare canopy conditions (Fig. 8). The contrast between snow-covered and snow-free conditions was much greater than the range in visible spectral albedo (0.03–0.04) observed for snow depths under the canopy ranging from 6.4 cm to 39.4 cm (Fig. 8). This suggests that forest albedo may not be very sensitive to underlying snow depth for deciduous broadleaf and mixed forests in this region, indicative of strong vegetation masking.

In the NIR region, spectral albedo was remarkably consistent across snow depths that ranged from 6.4 cm to 25.4 cm and SZA that ranged from 47° to 65°, with the exception of the 2013-02-10 spectrum (39.4 cm snow depth, 57° SZA), in which spectral albedo was 0.08–0.09 higher at wavelengths 1200–1350 nm. The higher NIR albedo on 2013-02-10 could be indicative of smaller grain sizes and lower liquid water content, given the low density of the snowpack (178 kg m^{-3}) compared to the other sampling dates when snow density ranged from 285 kg m^{-3} to 448 kg m^{-3} (Table 2). The decrease in NIR albedo with increasing snow density suggests that changes in grain size and or presence of liquid water and melting on the snowpack could be detectable through a forest canopy. More detailed measurements of grain size, liquid water, and melting would be necessary to confirm this. The snow-free spectrum collected on 2013-03-19 showed a decrease in visible spectrum albedo (−0.10 to −0.12) compared to snow-covered conditions, while NIR snow-free albedo increased at wavelengths greater than 1150 nm compared to days with snow cover (Fig. 8).

4.2.3. Tower-based and HSI shortwave broadband albedo

Mean spatially averaged 5 m HSI shortwave broadband albedo fell within ±0.04 at the TF Pasture site. At the TFP site, mean CMA6 tower-based albedo (0.71) was higher than HSI mean albedo (0.67) and comparable to snow-covered grassland (0.75) in Saskatchewan, Canada reported in Betts and Ball (1997).

At the TF Canopy and BF canopy validation sites mean HSI albedo fell within ±0.02 of the tower-based CMA6 measurements (0.17 to 0.19; Table 5). Forested values from the tower-based measurements were comparable to the Betts and Ball (1997) winter season averaged value of 0.21 reported over an aspen forest in Saskatchewan, Canada. Based on comparisons with ground- and tower-based ASD spectroradiometer observations of spectral albedo, HSI broadband albedo generally met the absolute accuracy requirement of ±0.05 for climate modeling (Henderson-Sellers & Wilson, 1983) over mixed forest, deciduous broadleaf forest, urban and built-up, and cropland/natural mosaic landscapes in New Hampshire.

Canopy shortwave broadband albedo increased by +0.04 to +0.08 when snow was present under the bare canopy compared to snow-free, bare canopy conditions (Table 2). However, none of the above-canopy spectra collected between 2012-03-08 and 2013-03-09 had snow on or within the canopy. Tower-based observations over a mixed deciduous broadleaf and evergreen needleleaf forest in Finland demonstrated an increase in shortwave broadband albedo (0.3–4.8 μm) of 0.2 for completely snow-covered canopy conditions with underlying snowpack compared to snow-free, dormant conditions (Kuusinen et al., 2012), a much larger increase than observed in this study (0.04 to 0.08; Table 2). Our results are in better agreement with the mean albedo change observed over a Saskatchewan aspen forest (0.09), in which dormant snow-free conditions were compared to a bare canopy with snow on the ground (Betts & Ball, 1997). Additional analysis of spectral albedo and shortwave broadband albedo of forest canopies with snow cover clinging to branches would be needed to determine the impact of canopy snow on forest albedo in the current study region.

4.3. HSI and MODIS comparison

4.3.1. HSI and MCD43A4 NBAR reflectance

For the 183 MODIS 500 m grid cells within the TF HSI study area, MCD43A4 NBAR root mean square errors (RMSEs) for bands 5–7 fell within ±0.04 of HSI reflectance values for the same spectral values, and were better than expected (±0.10) for poor quality magnitude inversions (Table 6). Band 3 (459–479 nm) generally had the highest RMSE's for all land cover types. The negative biases at shorter wavelengths could be linked to atmospheric artifacts caused by scattering

Table 6
Bias and root mean square error (RMSE) between of MCD43A4 magnitude inversion NBAR and HSI reflectance for MODIS bands 1–7, Thompson Farm Study Area.

Band	λ (nm)	Bias					RMSE				
		All pixels	Mixed forest	Decid. broadleaf	Urban & built-up	Cropland/natural mosaic	All pixels	Mixed forest	Decid. broadleaf	Urban & built-up	Cropland/natural mosaic
1	620–670	−0.027	−0.027	−0.017	0.013	0.140	0.090	0.080	0.094	0.079	0.140
2	841–876	−0.012	−0.009	0.003	0.007	0.104	0.064	0.053	0.083	0.052	0.104
3	459–479	−0.048	−0.049	−0.042	−0.002	−0.069	0.099	0.091	0.105	0.076	0.142
4	545–565	−0.018	−0.019	−0.012	0.024	0.133	0.087	0.077	0.099	0.080	0.133
5	1230–1250	0.020	0.020	0.034	0.022	0.020	0.025	0.024	0.042	0.024	0.020
6	1628–1652	0.002	0.002	0.008	0.001	0.013	0.010	0.009	0.017	0.006	0.013
7	2105–2155	−0.005	−0.005	−0.001	0.003	0.009	0.008	0.008	0.009	0.001	0.009

Table 7
Comparison of HSI spatially aggregated 5-m shortwave broadband albedo to MCD43A3 magnitude inversion blue-sky albedo and MOD10A1 daily blue-sky albedo 500-m pixels within the TF HSI study area.

MCD12Q1 land cover	Study Area	α_{sw}			Bias		RMSE	
		HSI	MCD43A3	MOD10A1	MCD43A3	MOD10A1	MCD43A3	MOD10A1
Decid. broadleaf	TF	0.28	0.27	0.28	−0.009	−0.002	0.077	0.085
	BF	0.18	0.14	0.17	−0.036	−0.006	0.039	0.026
Mixed forest	TF	0.27	0.25	0.27	−0.020	−0.006	0.059	0.059
	BF	0.18	0.15	0.18	−0.035	−0.010	0.062	0.040
Cropland/natural mosaic	TF	0.43	0.39	0.43	−0.037	−0.0014	0.10	0.11
Urban & built-up	TF	0.31	0.32	0.34	0.017	0.037	0.056	0.067
All pixels	TF	–	–	–	−0.018	−0.001	0.067	0.070
	BF	–	–	–	−0.035	−0.010	0.057	0.036

of light by aerosols and water vapor between the airborne sensor and the satellite sensor or overcorrection for aerosols over snow targets (Vermote et al., 2002). We also note that the MCD43A4 was based on a single day observation using the V005 backup algorithm and therefore are flagged as poor quality. Furthermore, HSI reflectance data were not BRDF-adjusted and the observation footprint of MODIS (750 m to 800 m) does not necessarily match spatially inhomogeneous 500 m MODIS grid cell in which HSI data were spatially averaged, contributing to high RMSEs of MCD43A4 relative to HSI (Table 6).

4.3.2. MODIS and HSI broadband albedo

For the 183 MODIS 500 m grid cells within the TF HSI study area, the bias in MOD10A1 shortwave broadband albedo was lower (−0.001) than MCD43A3 magnitude inversion albedo (−0.018) relative to HSI albedo spatially averaged to 500 m MODIS pixels, however, the overall RMSE for MOD10A1 (0.070) was greater than MCD43A3 (0.067) (Table 7). Similar to TF, MOD10A1 biases at BF were lower than MCD43A3 (−0.035), however, RMSEs were lower for MOD10A1 (0.036) compared to MCD43A3.

MOD10A1 500-m daily snow albedo biases in were weaker than MCD43A3 for deciduous broadleaf and mixed forest (Table 7). The lower biases in MOD10A1 may be due to the assumption that forests are Lambertian reflectors in MOD10A1; furthermore HSI albedo is not BRDF-adjusted. In addition, the MCD43A3 retrieval for 2013-03-09 was flagged as poor quality because it only included one BRDF retrieval on the day of the HSI flight. It is probable that the biases over forest would be reduced if high quality, full inversion MCD43A3 data were available.

MCD43A3 and MOD10A1 shortwave broadband albedo generally fell within ±0.04 of spatially averaged HSI albedo for the mixed forest and deciduous broadleaf forest MCD12Q1 pixels at BF (Fig. 9). MCD43A3 falls within the expected ±0.10 for poor quality magnitude inversion products in the MCD43 general accuracy statement.

Over urban & built-up pixels, MOD10A1 had a much larger bias and RMSE than MCD43A3 (Table 7). RMSEs over cropland/natural mosaic were comparable for MOD10A1 and MCD43A3, though biases were substantially smaller for MOD10A1 than for MCD43A3. Among the land cover classes analyzed, cropland/natural mosaic had the greatest bias and RMSE. The poor agreement between HSI and MODIS shortwave broadband albedo for 'cropland/natural mosaic' pixels was not surprising, given the heterogeneous nature of this land cover class, which is assigned to MODIS pixels with no more than 60% of the total land area being classified as any other land cover class by MCD12Q1 algorithms. A mixture of bright snow-covered landscapes with contrasting dark forest canopies could contribute to less accurate MODIS albedo retrievals.

The MCD43A3 RMSEs relative to HSI in this study are higher than reported in previous studies that evaluated MCD43A3 over spatially representative tower sites for snow-covered forests (Table 8; Wang et al., 2014) though they are comparable to RMSEs of snow-covered agriculture/grassland land cover types (Table 8; Wang et al., 2014).

In our comparison of HSI and MCD43A3 V005 albedo, we identified higher RMSEs for snow-covered forests, ranging from 0.039 to 0.077, than the Wang et al. (2014) RMSE (0.025) for 1-day daily magnitude inversion MCD43A3 V005 product over spatially representative snow-covered forests (Table 8). Previous studies indicate that RMSEs generally decrease for a high quality full inversion compared to poor quality magnitude inversion products (Table 8; Wang et al., 2012, 2014). As such, one could expect that the RMSEs over heterogeneous landscapes such as those studied here would decrease for high quality (full inversion) MCD43A3 BRDF-adjusted albedo.

The higher RMSE reported in this study over cropland/natural mosaic (0.10) were nearly double the RMSE for grassland and cropland snow-covered landscapes in previous studies (Wang et al., 2014; Wright et al., 2014; Wang et al., 2012; Stroeve et al., 2013; Table 8). The higher RMSEs reported here for cropland/natural mosaic compared

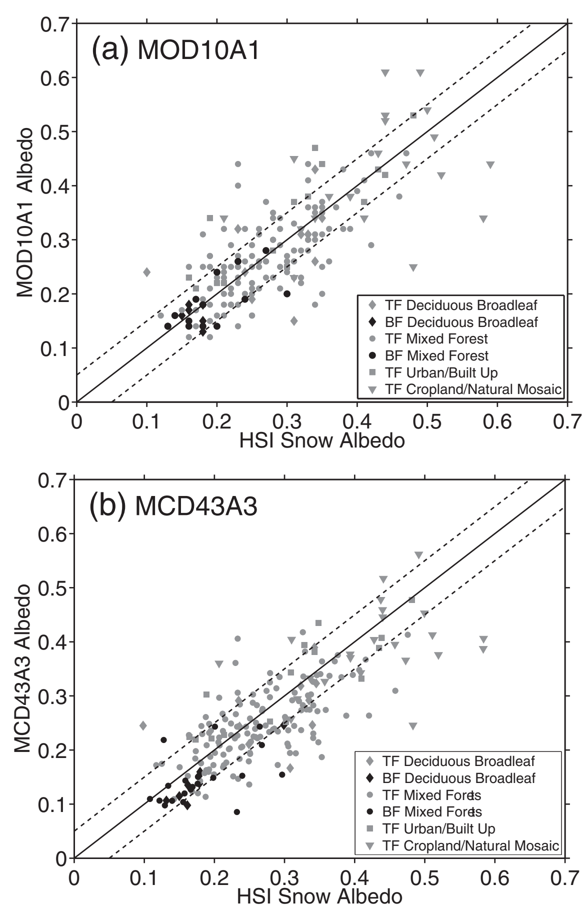

Fig. 9. Scatterplot of (a) MOD10A1 500-m daily broadband albedo and (b) MCD43A3 blue-sky albedo vs. HSI 5-m broadband albedo spatially aggregated to MODIS 500-m pixels at Thompson Farm (TF) and Bartlett Experimental Forest (BF). Solid black line is the 1:1 fit. Dashed lines represent ±0.05 absolute accuracy requirement described by Henderson-Sellers and Wilson (1983).

Table 8
RMSE and bias from previous MODIS snow albedo validation studies using MCD43A3 (terra and aqua combined).

Study	Land cover	MODIS dataset	RMSE	Bias
This study (BF)	Decid. broadleaf	MCD43A3 V005 1-day daily magnitude	0.039	−0.036
	Mixed forest	MCD43A3 V005 1-day daily magnitude	0.062	−0.035
This study (TF)	Decid. broadleaf	MCD43A3 V005 1-day daily magnitude	0.077	−0.009
	Mixed forest	MCD43A3 V005 1-day daily magnitude	0.059	−0.020
	Urban & built-up	MCD43A3 V005 1-day daily magnitude	0.056	+0.017
	Cropland/Natural Mosaic	MCD43A3 V005 1-day daily magnitude	0.100	−0.037
Wang et al. (2014)	Forest	MCD43A3 V005 1-day daily magnitude	0.025	±0.023
	Forest	MCD43A3 V005 16-day daily full	0.005	±0.005
	Forest	MCD43A3 V005 16-day daily magnitude	0.025	±0.023
	Forest	MCD43A3 V005 16-day standard full	0.005	±0.005
	Forest	MCD43A3 V005 16-day standard magnitude	0.025	±0.025
	Agriculture/grassland	MCD43A3 V005 1-day daily magnitude	0.041	±0.025
	Agriculture/grassland	MCD43A3 V005 16-day daily full	0.041	±0.027
	Agriculture/grassland	MCD43A3 V005 16-day daily magnitude	0.046	±0.026
	Agriculture/grassland	MCD43A3 V005 16-day standard full	0.022	±0.018
	Agriculture/grassland	MCD43A3 V005 16-day standard magnitude	0.050	±0.030
Wright et al. (2014)	Greenland ice sheet	MCD43A3 V005 DB full	0.033	+0.023
	Greenland ice sheet	MCD43A3 V005 DB full and magnitude	0.035	+0.027
	Greenland ice sheet	MCD43A3 V006	0.026	−0.015
Wang et al. (2012)	Tundra	MCD43A3 V005 1-day daily	0.033	±0.018
	Tundra	MCD43A3 V005 16-day daily	0.047	±0.024
	Tundra	MCD43A3 V005 16-day standard	0.045	±0.045
Stroeve et al. (2013)	Greenland ice sheet	MCD43A3 V005 16-day standard, full	0.067	+0.022

to previous studies were likely due to a combination of fewer available cloud-free days available for local magnitude inversion (flagged as poor quality) and the high spatial heterogeneity in our study area and because this land cover class has a variable range in area of exposed snow that is more sensitive to BRDF corrections used in the magnitude inversion to account for anisotropy in both MOD10A1 and MCD43A3.

5. Conclusions and future work

This study spatially scaled ground- and tower-based and airborne HSI to MODIS reflectance quantities over mixed forest, deciduous broadleaf forest, urban and built-up, and cropland/natural mosaic snow-covered landscapes in New Hampshire, USA. The ground validation of HSI radiance, HCRF, spectral and shortwave broadband albedo demonstrated that high resolution HSI data is well suited for providing accurate albedo over forested and mixed-landscapes in the presence of snow and scaling to coarser resolution remote sensing products such as MODIS. Spectral albedo of snow-covered pasture was underestimated by HSI relative to ground-based measurements in the visible part of the spectrum and was strongly underestimated – by up to −0.5 – at wavelengths less than 450 nm. We attributed this to atmospheric absorption artifacts and recommend that future efforts on remote sensing of albedo over snow-covered surfaces focus on improving atmospheric corrections in this portion of the spectrum. Such efforts would be valuable for better prediction of surface albedo over snow-covered surfaces and modeling climate responses to snow-cover dynamics.

HSI surface reflectance and albedo over a bare deciduous broadleaf canopy with underlying snow cover in New Hampshire agreed well with tower-based measurements and generally met the absolute accuracy requirement of ±0.05 recommended for climate modeling (Henderson-Sellers & Wilson, 1983).

Currently, Coupled Model Intercomparison Project (CMIP5) models exhibit a five-fold spread in the change in surface snow albedo associated with a 1 °C change in surface air temperature, predominantly due to varying treatments of vegetation masking of snow by forest canopies (Qu & Hall, 2014). The research presented here demonstrates that variations in snow depth under the canopy do not influence canopy albedo by more than ±0.04 and that the presence of snow under the canopy increases albedo by at most +0.08. This suggests strong vegetation masking of snow in the study region though additional research is necessary to understand the duration and influence of canopy snow on surface albedo. This could help to improve parameterization of surface albedo for temperature deciduous broadleaf and mixed forests during periods of snow cover in land surface models used by global climate models (GCMs). The tower-based spectral albedo measurements and HSI albedo collected over forest canopies during dormant, snow-free conditions and with snow under the canopy will also contribute to more accurate evaluation of spectral remote sensing products (e.g., Suomi-NPP VIIRS, Landsat-8/OLI, Sentinel-2, and HyspIRI) and expand existing spectral libraries used in detection and modeling of surface reflectance properties.

This study demonstrated that both MCD43A3 albedo and MOD10A1 snow albedo performed well over forested landscapes relative to HSI albedo data that had been validated with ground-based measurements, with biases less than ±0.04 for the four IGBP land cover classes evaluated (deciduous broadleaf, mixed forest, cropland/natural mosaic, and urban & built-up). In general, the MCD43A3 poor quality magnitude inversion product performed better than expected; the RMSEs reported here were greater than previously reported high quality, full inversion products over spatially representative validation sites. MOD10A1 daily snow albedo product biases and RMSEs relative to HSI were lower than poor-quality MCD43A3 BRDF-adjusted albedo product over deciduous broadleaf forest, mixed forest, and cropland/natural mosaic. Over urban & built-up land cover, poor quality MCD43A3 performed better than MOD10A1. Evaluation of the key differences in MODIS daily snow albedo products warrants further investigation over a range of snow conditions and forest compositions given that the conclusions presented in this study are based on relatively poor quality MCD43A3 local magnitude inversion albedo product.

Acknowledgments

This research was supported by the New Hampshire Ecosystems and Society National Science Foundation Experimental Program to Stimulate Competitive Research (Award EPS-1101245), the National Aeronautic and Space Administration Terrestrial Ecology Program (Grant #NNX11AB88G), and the NSF (DEB#0832652) Hubbard Brook Long Term Ecological Research (LTER) project. The use of the ASD FieldSpec4 in March 2012 was provided by the Alexander Goetz Instrument Fellowship Program (2011/2012). The authors would also like to thank the Richardson Lab at Harvard University for loan of an ASD spectroradiometer on 2013-03-09. The authors thank the USDA-Forest Service for loan of the Kipp and Zonen CMA6 at Thompson Farm

Research Station, and Bob Evans of the USDA Forest Service for technical assistance.

References

Betts, A.K., & Ball, J.H. (1997). Albedo over the boreal forest. *Journal of Geophysical Research*, *102*, 28901–28909.

Bonan, G. (2008). Forests and climate change: Forcings, feedbacks, and the climate benefits of forests. *Science*, *320*, 1444–1449.

Carroll, S.S., & Cressie, N. (1996). A comparison of geostatistical methodologies used to estimate snow water equivalent. *Water Resources Bulletin*, *32*, 267–278.

Friedl, M.A., McIver, D.K., Hodges, J.C.F., Zhang, X.Y., Muchoney, D., Strahler, A.H., Woodcock, C.E., Gopal, S., Schneider, A., Cooper, A., Baccini, A., Gao, F., & Schaaf, C.B. (2002). Global Land Cover Mapping from MODIS: Algorithms and early results. *Remote Sensing of Environment*, *83*, 287–302.

Friedl, M.A., Sulla-Menashe, D., Tan, B., Schneider, A., Ramankutty, N., Sibley, A., & Huang, X. (2010). MODIS Collection 5 global land cover: Algorithm refinements and characterization of new datasets. *Remote Sensing of Environment*, *114*, 168–182.

Gueymard, C. (1995). *SMARTS, A Simple Model of the Atmospheric Radiative Transfer of Sunshine: Algorithms and performance assessment. Professional paper FSEC-PF-270-95.* 1679 Clearlake Rd, Cocoa, FL: Florida Solar Energy Center, 32922.

Gueymard, C. (2001). Parameterized transmittance model for direct beam and circumsolar spectral irradiance. *Solar Energy*, *71*, 325–346.

Hall, D.K., Nghiem, S.V., Schaaf, C.B., DiGirolamo, N.E., & Neumann, G. (2009a). Evaluation of surface and near-surface melt characteristics on the Greenland ice sheet using MODIS and QuikSCAT data. *Journal of Geophysical Research*, *114*, F04006, http://dx.doi.org/10.1029/2009JF001287.

Hall, D.K., & Riggs, G.A. (2007). Accuracy assessment of the MODIS snow products. *Hydrological Processes*, *21*, 1534–1547, http://dx.doi.org/10.1002/hyp.6715.

Hall, D.K., Salomonson, V.V., & Riggs, G.A. (2006). *MODIS/Terra Snow Cover Daily L3 Global 500 m Grid. Version 5. [Granule ID: MOD10A1.A2013068.h12v04.005.2013070055015.hdf].* Boulder, Colorado USA: National Snow and Ice Data Center.

Hall, D.K., Schaaf, C.B., Wang, Z., & Riggs, G.A. (2009, Januaryb). Enhancement of the MODIS daily snow albedo product. *Paper presented at the 89th Annual Meeting of the American Meteorological Society* (pp. 11–15) (Phoenix, AZ).

Hayhoe, K., Wake, C.P., Huntington, T.G., Luo, L., Schwartz, M.D., Sheffield, J., Wood, E., Anderson, B., Bradbury, J., DeGaetano, A., Troy, T.J., & Wolfe, D. (2007). Past and future changes in climate and hydrological indicators in the US Northeast. *Climate Dynamics*, *28*, 381–407, http://dx.doi.org/10.1007/s00382-006-0187-8.

Henderson-Sellers, A., & Wilson, M.F. (1983). Surface albedo data for climatic modeling. *Review of Geophysics*, *21*, 1743–1778.

Jin, Y., Schaaf, C.B., Gao, F., Li, X., & Strahler, A.H. (2003a). Consistency of MODIS surface bidirectional reflectance distribution function and albedo retrievals: 1. Algorithm performance. *Journal of Geophysical Research*, *108*(D5), 4158, http://dx.doi.org/10.1029/2002JD002803.

Jin, Y., Schaaf, C.B., Woodcock, C.E., Gao, F., Li, X., & Strahler, A.H. (2003b). Consistency of MODIS surface bidirectional reflectance distribution function and albedo retrievals: 2. Validation. *Journal of Geophysical Research*, *108*(D5), 4159, http://dx.doi.org/10.1029/2002JD002804.

Klein, A.G., Hall, D.K., & Riggs, G.A. (1998). Improving snow cover mapping in forests through the use of a canopy reflectance model. *Hydrological Processes*, *12*, 1723–1744.

Klein, A.G., & Stroeve, J.C. (2002). Development and validation of a snow albedo algorithm for the MODIS instrument. *Annals of Glaciology*, *34*, 45–52.

Kotchenova, S.Y., Vermote, E.F., Matarrese, R., & Klemm, F.J. (2006). Validation of a vector version of the 6 s radiative transfer code for atmospheric correction of satellite data. Part I: Path radiance. *Applied Optics*, *45*, 6726–6774.

Kuusinen, N., Kolari, P., Levula, J., Porcar-Castell, A., Stenberg, P., & Berninger, F. (2012). Seasonal variation in boreal pine forest albedo and effects of canopy snow on forest reflectance. *Agricultural and Forest Meteorology*, *164*, 53–60.

Liang, S.L. (2001). Narrowband to broadband conversions of land surface albedo I. Algorithms. *Remote Sensing of Environment*, *76*, 213–238.

Liu, J., Schaaf, C.B., Strahler, A.H., Jiao, Z., Shuai, Y., & Zhang, Q. (2009). Validation of Moderate Resolution Imaging Spectroradiometer (MODIS) albedo retrieval algorithm: Dependence of albedo on solar zenith angle. *Journal of Geophysical Research-Atmospheres*, *114*, D01106, http://dx.doi.org/10.1029/2008JD009969.

Michalsky, J.J., Harrison, L.C., & Berheiser, W.E., III (1995). Cosine response characteristics of some radiometric and photometric sensors. *Solar Energy*, *54*(6), 397–402.

Mote, T.L. (2008). On the role of snow cover in depressing air temperature. *Journal of Applied Meteorology and Climatology*, *47*, 2008–2022.

National Operational Hydrologic Remote Sensing Center (NOHRSC) (2004). *Snow Data Assimilation System (SNODAS) data products at NSIDC.* Boulder, CO: National Snow and Ice Data Center. Digital media.

Noreus, J.P., Nyborg, M.R., & Hayling, K.L. (1997). The gravity anomaly field in the Gulf of Bothnia spatially characterized from satellite altimetry and in situ measurements. *Journal of Applied Geophysics*, *37*, 67–84.

Perron, C.J., Bennett, K., & Lee, T.D. (2004). *Forest stewardship plan: Thompson farm.* NH: University of New Hampshire. Produced by Ossipee Mountain Land Company, West Ossipee (Downloaded 2013-04-02: https://colsa.unh.edu/woodlands/sites/colsa.unh.edu.woodlands/files/docs/Thompson_Farm.pdf).

Qu, X., & Hall, A. (2006). Assessing snow albedo feedback in simulated climate change. *Journal of Climate*, *19*, 2617–2630.

Qu, X., & Hall, A. (2014). On the persistent spread in snow-albedo feedback. *Climate Dynamics*, *42*, 69–81, http://dx.doi.org/10.1007/s00382-013-1774-0.

Riggs, G. A., Hall, D.K., & Salomonson, V.V. (2006). *MODIS Snow Products User Guide to Collection 5.* (Accessed 2011–05–10: http://modis-snow-ice.gsfc.nasa.gov/uploads/sug_c5.pdf).

Román, M.O., Schaaf, C.B., Lewis, P., Gao, F., Anderson, G.P., Privette, J.L., Strahler, A.H., Woodcock, C.E., & Barnsley, M. (2010). Assessing the coupling between surface albedo derived from MODIS and the fraction of diffuse skylight over spatially-characterized landscapes. *Remote Sensing of Environment*, *114*, 738–760.

Román, M.O., Schaaf, C.B., Woodcock, C.E., Strahler, A.H., Yang, X., Braswell, R.H., Curtis, P.S., Davis, K.J., Dragoni, D., Goulden, M.L., Gu, L., Hollinger, D.Y., Kolb, T.E., Meyers, T.P., Munger, J.W., Privette, J.L., Richardson, A.D., Wilson, T.B., & Wofsy, S.C. (2009). *Remote Sensing of Environment*, *113*, 2476–2498.

Salomon, J.G., Schaaf, C.B., Strahler, A.H., Gao, F., & Jin, Y. (2006). Validation of the MODIS bidirectional reflectance distribution function and albedo retrievals using combined observations from the aqua and terra platforms. *IEEE Transactions on Geoscience and Remote Sensing*, *44*(6), 1555–1565.

Schaaf, C.B., Gao, F., Strahler, A.H., Lucht, W., Li, X., Tsang, T., Strugnell, N.C., Zhang, X., Jin, Y., Muller, J. -P., Lewis, P., Barnsley, M., Hobson, P., Disney, M., Roberts, G., Dunderdale, M., Dol, C., d'Entremont, R.P., Hu, B., Liang, S., Privette, J.L., & Roy, D. (2002). First operational BRDF, albedo nadir reflectance products from MODIS. *Remote Sensing of Environment*, *83*, 135–148.

Schaaf, C.L.B., Liu, J., Gao, F., & Strahler, A.H. (2011). MODIS albedo and reflectance anisotropy products from aqua and terra. In B. Ramachandran, C. Justice, & M. Abrams (Eds.), *Land remote sensing and global environmental change: NASA's Earth Observing System and the Science of ASTER and MODIS. Remote Sensing and Digital Image Processing Series*, *11*, . Springer-Cerlag (873 pp.).

Schaaf, C. B., Martonchik, J., Pinty, B., Govaerts, Y., Gao, F., Lattanzio, A., et al. (2008). Retrieval of surface albedo from satellite sensors. In S.Liang (Ed.), *Advances in land remote sensing: System, modeling, inversion and application*, 219–243 Springer.

Schaepman-Strub, G., Schaepman, M.E., Painter, T.H., Dangel, S., & Martonchik, J.V. (2006). Reflectance quantities in optical remote sensing — Definitions and case studies. *Remote Sensing of Environment*, *103*, 27–42.

Shuai, Y., Masek, J.G., Gao, F., & Schaaf, C.B. (2011). An algorithm for the retrieval of 30-m snow-free albedo from MODIS BRDF and Landsat surface reflectance. *Remote Sensing of Environment*, *115*, 2204–2216.

Stroeve, J.C., Box, J.E., Gao, F., Liang, S., Nolin, A., & Schaaf, C.B. (2005). Accuracy assessment of the MODIS 16-day albedo product for snow: Comparisons with Greenland in situ measurements. *Remote Sensing of Environment*, *94*, 46–60.

Stroeve, J.C., Box, J.E., & Haran, T. (2006). Evaluation of the MODIS (MOD10A1) daily snow albedo product over the Greenland ice sheet. *Remote Sensing of Environment*, *105*, 155–181.

Stroeve, J.C., Box, J.E., Wang, Z., Schaaf, C.B., & Barrett, A. (2013). Re-evaluation of MODIS MCD43 Greenland albedo accuracy and trends. *Remote Sensing of Environment*, *138*, 199–214.

Tekeli, A.E., Şensoy, A., Şorman, A., Akyürek, Z., & Şorman, Ü. (2006). Accuracy assessment of MODIS daily snow albedo retrievals with *in situ* measurements in Karasu Basin, Turkey. *Hydrological Processes*, *20*, 705–721.

Vermote, E.F., El Saleous, N.Z., & Justice, C.O. (2002). Atmospheric correction of MODIS data in the visible to middle infrared: First results. *Remote Sensing of Environment*, *83*, 97–111.

Vermote, E.F., El Saleous, N.Z., Justice, C.O., Kaufman, Y.J., Privette, J.L., Remer, L., et al. (1997). Atmospheric correction of visible to middle infrared EOS-MODIS data over land surfaces: Background, operational algorithm, and validation. *Journal of Geophysical Research*, *102*, 17131–17141.

Wang, Z., Schaaf, C.B., Chopping, M.J., Strahler, A.H., Wang, J., Román, M.O., Rocha, A.V., Woodcock, C.E., & Shuai, Y. (2012). Evaluation of Moderate-resolution Imaging Spectroradiometer (MODIS) snow albedo product (MCD43A) over tundra. *Remote Sensing of Environment*, *117*, 264–280, http://dx.doi.org/10.1016/j.rse.2011.10.002.

Wang, Z., Schaaf, C.B., Strahler, A.H., Chopping, M.J., Román, M.O., Shuai, Y., Woodcock, C.E., Hollinger, D.Y., & Fitzjarrald, D.R. (2014). Evaluation of MODIS albedo product (MCD43A over grassland, agriculture and forest surface types during dormant and snow-covered periods. *Remote Sensing of Environment*, *140*, 60–77.

Warren, S.G. (1982). Optical properties of snow. *Reviews of Geophysics and Space Physics*, *20*(1), 67–89.

Wolfe, R.E., Nishihama, M., Fleig, A.J., Kuyper, J.A., Roy, D.P., Storey, J.C., & Patt, F.S. (2002). Achieving sub-pixel geolocation accuracy in support of MODIS land science. *Remote Sensing of Environment*, *83*, 31–49.

Wright, P., Bergin, M., Dibb, J.E., Lefer, B., Domine, F., Carman, T., Carmagnola, C., Dumont, M., Courville, Z., Schaaf, C.B., & Wang, Z. (2014). Comparing MODIS daily snow albedo to spectral albedo field measurements in Central Greenland. *Remote Sensing of Environment*, *140*, 118–129, http://dx.doi.org/10.1016/j.rse.2013.08.044.